Climate change trend in China, with improved accuracy

**Tian-Xiang Yue · Na Zhao · R. Douglas Ramsey ·
Chen-Liang Wang · Ze-Meng Fan · Chuan-Fa Chen ·
Yi-Min Lu · Bai-Lian Li**

Abstract We have found that a spatial interpolation of mean annual temperature (MAT) in China can be accomplished using a global ordinary least squares regression model since the relationship between temperature and its environmental determinants is constant. Therefore the estimation of MAT does not very across space and thus exhibits spatial stationarity. The interpolation of mean annual precipitation (MAP), however, is more complex and changes spatially as a function of topographic variation. Therefore, MAP shows spatial non-stationarity and must be estimated with a geographically weighted regression. A statistical transfer function (STF) of MAT was formulated using minimized residuals output from a high accuracy and high speed method for surface modeling (HASM) with an ordinary least squares (OLS) linear equation that uses latitude and elevation as independent variables, abbreviated as HASM-OLS. The STF of MAP under a BOX-COX transformation is derived as a combination of minimized residuals output by HASM with a geographically weighted regression (GWR) using latitude, longitude, elevation, impact coefficient of aspect and sky view factor as independent variables, abbreviated as HASM-GWR-BC. In terms of HASM-OLS and HASM-GWR-BC,

T.-X. Yue (✉) · N. Zhao · C.-L. Wang · Z.-M. Fan
State Key Laboratory of Resources and Environment Information System, Institute of Geographical Science and Natural Resources Research, Chinese Academy of Sciences, 11A, Datun Road, Anwai, 100101 Beijing, China
e-mail: yue@lreis.ac.cn

C.-F. Chen
Geomatics College, Shandong University of Science and Technology
266510 Qingdao, Shandong Province, China

R. D. Ramsey
Department of Wildland Resources, Utah State University, Logan, UT 84322-5230, USA

Y.-M. Lu
Key Lab of Spatial Data Mining and Information Sharing, Fuzhou University
No. 523, Gongye Road, 350002 Fuzhou, China

T.-X. Yue · B.-L. Li
Ecological Complexity and Modeling Laboratory, University of California
Riverside, CA 92521, USA

MAT had an increasing trend since the 1960s in China, with an especially accelerated increasing trend since 1980. Overall, our data show that MAT has increased by 1.44 °C since the 1960s. The warming rates increase from the south to north in China, except in the Qinghai-Xizang plateau. Specifically, the 2,100 °C·d contour line of annual accumulated temperature (AAT) of ≥10 °C shifted northwestward 255 km in the Heilongjiang province since the 1960s. MAP in Qinghai-Xizang plateau and in arid region had a continuously increasing trend. In the other 7 regions of China, MAP shows both increasing and decreasing trends. On average, China became wetter from the 1960s to the 1990s, but drier from the 1990s to 2000s. The Qinghai-Xizang Plateau and Northern China experienced more climatic extremes than Southern China since the 1960s.

1 Introduction

Meteorological stations are primary sources for climatic data. However, sparsely distributed meteorological stations are often unable to satisfy the data requirements of most ecosystem change studies. One major problem is how to estimate values for locations where primary data is not available (Akinyemi and Adejuwon 2008).

GIS-based techniques have been widely used for interpolating observed point-based climatic data (Agnew and Palutikof 2000; Yue 2011). For instance, Ordinary kriging (OK) was used to interpolate the daily and monthly rainfall of Australia using ground-based observational data (Jeffrey et al. 2001). Lloyd (2005) compared the performance of different interpolation methods, including a moving window regression (MWR), inverse distance weighting (IDW) and Kriging, demonstrating that methods using elevation as secondary data performed better than others because of the relationships between climate factors, such as temperature, precipitation and evaporation, to elevation. Hancock and Hutchinson (2006) used thin plate smoothing splines (Spline) to interpolate mean annual temperature of the Australian and African continents.

Thiessen polygons (TP), IDW, Spline and OK were used to interpolate thirteen widely scattered rainfall stations and their daily time series into gridded rainfall surfaces over the 1950–1992 period in a West African catchment; assessment of the interpolation methods using reference point data indicated that interpolations using the IDW and OK were more efficient than TP and, to a lesser extent, Spline (Ruelland et al. 2008). Different interpolation models in a GIS environment were used to generate precipitation surfaces for the north-western Himalayan Mountains and upper Indus plains of Pakistan at a spatial resolution of 250×250 m^2 for a baseline period (1960–1990). This precipitation simulation using a regional climate model (PRECIS) showed that OK, using elevation as secondary data, provided the best results especially for the monsoon months (Ashiq et al. 2010). Three interpolation approaches, IDW, Spline and Co-kriging, were used to interpolate monthly mean temperature, seasonal mean temperature, and annual mean temperature in the eastern part of India; it was found that Spline was preferred to Kriging and IDW because it was faster and easier to use (Samanta et al. 2012).

Many scholars are working to improve the interpolation of climate surfaces by using data from meteorological stations in China. For instance, Shang et al. (2001) employed IDW to interpolate mean annual precipitation from 1951 to 1980, including a digital elevation model (DEM) as secondary data; the interpolation had a mean absolute error of 102.23 mm. Lin et al. (2002) applied different interpolation techniques, OK and IDW, to estimate 10-day mean air temperature from 1951 to 1990; the results indicated that the mean absolute errors for OK and IDW were 2.15 °C and 1.9 °C respectively. Pan et al. (2004) interpolated mean annual temperature using 726 meteorological station observations in China from 1961 to 2000

using IDW with a mean absolute error of 1.51 °C. Hong et al. (2005) used climate data from 1971 to 2000 from meteorological stations in China to develop thin-plate smoothing spline surfaces for monthly mean temperature and precipitation for January, April, July and October. Their results showed interpolation errors for monthly temperatures varying from 0.42 to 0.83 °C and 8–13 % for monthly precipitation.

A combination of interpolation methods applied through statistical transfer functions (STFs) is an efficient approach to improve the estimation error of climatic variables for locations where primary data is not available. It has been determined that the statistical relationship between mean annual temperature (MAT) and its environmental determinants is the same no matter where the measurement takes place (Yue 2011). But a simple 'global' model cannot explain the relationship between mean annual precipitation (MAP) and its environmental variables. The MAP relationship changes across space as a function of topographic structure across the landscape. In other words, MAT exhibits spatial stationarity and its statistical transfer function can be expressed by an Ordinary Least Squares regression (OLS), while MAP exhibits spatial non-stationarity and therefore its statistical transfer functions have to be formulated through Geographically Weighted Regression (GWR). In this paper, OLS for MAT and GWR for MAP are combined with a high accuracy and high speed method for surface modeling (HASM) to produce surfaces of climatic change for the past 50 years in China at a spatial resolution of 1 km×1 km. HASM, OLS and GWR are described in detail by the online supplements 1 and 2.

2 Methods

A STF of MAT was formulated using minimized residuals output from HASM with an OLS linear equation that used latitude and elevation as independent variables. This MAT transfer function is abbreviated as HASM-OLS (Supplement 2). The simulated MAT from 1961 to 2010 at every grid cell i, in which i=1, 2,…, 19606916, can be formulated as,

$$Ts_i(t) = \theta_{ols} \cdot \mathbf{x}^T + HASM\left(T_k(t) - \theta_{ols} \cdot \mathbf{x}^T\right) \tag{1}$$

where $\mathbf{x}$=(1, Lat, Ele), $\boldsymbol{\theta}_{ols}$=(38.552, 0.705, 0.003), $T_k(t)$ is the MAT observed in the year of t at the meteorological station k.

The STF of MAP under a BOX-COX transformation was derived as a combination of minimized residuals output by HASM with a GWR using latitude, longitude, elevation, impact coefficient of aspect and sky view factor as independent variables. The MAP transfer function is abbreviated as HASM-GWR-BC (Supplement 2). Let $\mathbf{x}$=(Lon, Lat, Ele, ICA, SVF), in which Lat represents latitude, Lon refers to longitude, Ele is elevation, ICA the impact coefficient of aspect on precipitation, and SVF the sky view factor. Then the STF of MAP under a BOX-COX transformation can be formulated as,

$$Ps_i(t) = \boldsymbol{\theta}_{gwr} \cdot \mathbf{x}^T + HASM\left(\Psi_{0.475}(P_k(t)) - \boldsymbol{\theta}_{gwr} \cdot \mathbf{x}^T\right) \tag{2}$$

where θ_{gwr}=$(\mathbf{x} \cdot \mathbf{W} \cdot \mathbf{x}^T)^{-1} \cdot \mathbf{x} \cdot \mathbf{W} \cdot \Psi_{0.475}(P_k(t))$; $\mathbf{W}$ is the geographical weight matrix; Ps_i is the simulated MAP at the grid cell i(i=1, 2,…,19606916); $\Psi_{0.475}(P_k(t))$=$(P_k^{0.475}(t)-1)/0.475$ is a BOX-COX transformation of annual mean precipitation $P_k(t)$ at observation station k in the year t.

Results of the HASM-OLS of MAT and HASM-GWR-BC of MAP were cross-validated using observational data from meteorological stations across China for the same period, for

which mean absolute error (MAE) and mean relative error (MRE) of climate variables are calculated. They are respectively formulated as,

$$MAE = \frac{1}{n} \sum_{i}^{n} |o_i - s_i| \tag{3}$$

$$MRE = \frac{MAE}{\frac{1}{n} \sum_{i=1}^{n} |o_i|} \times 100\% \tag{4}$$

where o_i represents the observed value such as MAT or MAP at the ith meteorological station; s_i the simulated value at the ith meteorological station; n is the total number of meteorological stations for validation.

We used a consistent cross-validation methodology to test OK, IDW, Spline, and HASM results. Validation results of HASM-OLS for MAT during the 1961 to 2010 period were compared to the OK-OLS, IDW-OLS and Spline-OLS results. OK-OLS, IDW-OLS and Spline-OLS respectively refer to the combination of OK, IDW and Spline with the OLS. GWR-BC means that the result of a BOX-COX transformation of MAP during the 1961 to 2010 period at every meteorological station were used to operate the geographically weighted regression. HASM-GWR-BC, OK-GWR-BC, IDW-GWR-BC and Spline-GWR-BC respectively describe the interpolation processes of MAP by combining HASM, OK, IDW and Spline with GWR-BC.

2.1 Cross-validation in space

Cross-validation in space was comprised of four steps: i) 5 % of the meteorological stations were removed for validation prior to model creation; ii) MAT and MAP from 1961 to 2010 were simulated at a spatial resolution of $1\,km \times 1\,km$ using the remaining 95 % of meteorological stations, iii) MAE and MRE were calculated using the 5 % validation set, and iv) the 5 % validation set is returned to the pool of available station for the next iteration. This process is repeated until MAT and MAP at all meteorological stations have been simulated and the simulation error statistics for each station can be calculated.

Cross validation in space indicates that MAEs of MAT during the 1961 to 2010 period created by HASM-OLS, OK-OLS,IDW-OLS and Spline-OLS were 0.73 °C, 0.81 °C, 0.82 °C and 1.18 °C respectively. MAT accuracy of HASM-OLS was 11 %, 12 % and 62 % higher than OK-OLS, IDW-OLS and Spline-OLS respectively. MAEs of MAP during the 1961 to 2010 period produced by HASM-GWR-BC, OK-GWR-BC, IDW-GWR-BC and Spline-GWR-BC are 48.78 mm, 65.29 mm, 65.10 mm and 124.14 mm respectively (Table 1). MAP accuracy of HASM-GWR-BC was 34 %, 34 % and 155 % greater than the accuracies of OK-GWR-BC, IDW-GWR-BC and Spline-GWR-BC respectively. HASM was the best performer when compared to the more widely used classical methods.

Results from Pan et al. (2004) and Shang et al. (2001) indicated that the interpolation results of MAT and MAP had MREs of 13 % and 14 % using IDW (Table 1). In other words, the accuracies of MAT and MAP interpolation were respectively increased by 6 % and 3 % because of the introduction of the STFs.

Table 1 Cross-validation in space

Mean annual temperature (°C)			Mean annual precipitation (mm)		
Method	MAE (°C)	MRE (%)	Methods	MAE (mm)	MRE (%)
HASM-OLS	0.73	6	HASM- GWR-BC	48.78	8
OK-OLS	0.81	7	OK- GWR-BC	65.29	11
IDW-OLS	0.82	7	IDW- GWR-BC	65.10	11
SPLINE-OLS	1.18	10	SPLINE- GWR-BC	124.14	17
IDW (Pan et al. 2004)	1.51	13	IDW (Shang et al. 2001)	102.23	14

2.2 Cross-validation in time

We used MAT and MAP from the 661 meteorological stations within 5 years, randomly selected from all years from the 50 year record, as the validation source, while the remaining data was used for model calibration. In other words, first, MAT and MAP were simulated at a spatial resolution of $1\,km \times 1\,km$ using data from the 661 meteorological stations for the other 45 years; then, MAE and MRE were calculated using the 5-year validation data; the validation data was then returned to the pool of available MAT and MAP measurements. This process is repeated until MAT and MAP for all 50 years was simulated and error statistics for each simulation calculated (Table 2).

The cross-validation in time demonstrated that MAEs of MAT, created by HASM-OLS, OK-OLS,IDW-OLS and Spline-OLS, were respectively 0.75 °C, 0.95 °C, 0.79 °C and 0.81 °C. MRE of HASM-OLS was 3 %, 2 % and 2 % lower than OK-OLS, IDW-OLS and Spline-OLS respectively. MAEs of MAP produced by HASM-GWR-BC, OK-GWR-BC, IDW-GWR-BC and Spline-GWR-BC are 89.29 mm, 98.08 mm, 93.17 mm and 143.23 mm respectively (Table 2). MRE of HASM-GWR-BC was 6 %, 4 % and 8 % smaller than OK-GWR-BC, IDW-GWR-BC and Spline-GWR-BC respectively. HASM had the highest accuracy when compared to the widely used classic methods.

3 Climatic change trend

A zoning system dividing the land mass of China into 9 regions with similar temperature, precipitation and soil regimes was adopted to make it easier to analyze changes in precipitation and temperature from one place to another (Zhou et al. 1981). The 9 regions are respectively termed as R_i, i=1, 2, …, 9 (Fig. 1).

Table 2 Cross-validation in time

Mean annual temperature (°C)			Mean annual precipitation (mm)		
Method	MAE (°C)	MRE (%)	Methods	MAE (mm)	MRE (%)
HASM-OLS	0.75	6	HASM- GWR-BC	89.29	14
OK-OLS	0.95	9	OK- GWR-BC	98.08	20
IDW-OLS	0.79	8	IDW- GWR-BC	93.17	18
SPLINE-OLS	0.81	8	SPLINE- GWR-BC	143.23	22
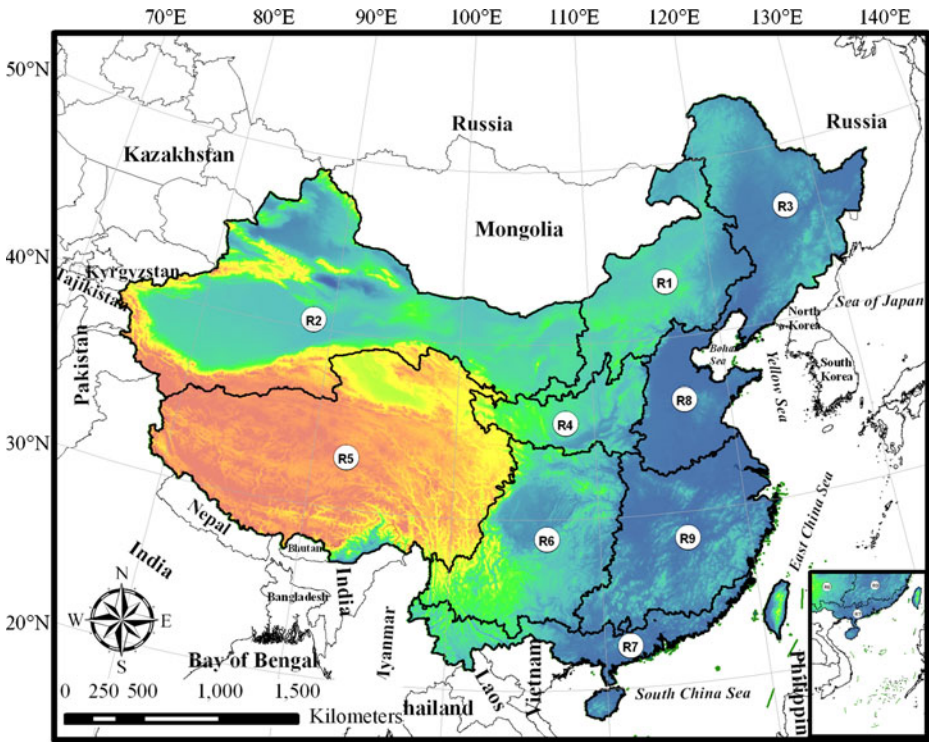
Fig. 1 Digital elevation model and 9 regions of China

3.1 Mean annual temperature

Annual temperature on average (ATOA) has generally shown an increasing trend in China from 1961 to 2010 (Fig. 2) with an average decadal increasing rate of 0.33 °C. The linear regression equation of the entire time series of ATOA, with correlation coefficient of 0.85 and significance level of 0.001, can be expressed as,

$$Tem(t) = 0.033t - 58.33 \qquad (5)$$

where *Tem(t)* is ATOA at the time of *t*; *t*=1, 2,…, 49, 50 represents the year of 1961, 1962, …, 2009 and 2010 respectively.

The significance level of 0.001 implies that there's only one chance in a thousand this could have happened by coincidence. The lower the significance level chosen, the stronger the evidence required. Smaller levels of significance level increase confidence in the determination of significance.

The period from 1961 to 2010 can be divided into 5 sub-periods: C_1 (from 1961 to 1970), C_2 (from 1971 to 1980), C_3 (from 1981 to 1990), C_4 (from 1991 to 2000) and C_5 (from 2001 to 2010). MATs during the sub-periods of C_1, C_2, C_3, C_4 and C_5 are respectively 6.91 °C, 7.15 °C, 7.33 °C, 7.82 °C and 8.35 °C. The changes of MATs are summarized in Table 3 where $\Delta C21$ represents the result of subtracting the value of MAT in C_1 from the value of the MAT in C_2, $\Delta C32$ represents the result of subtracting the value of the MAT in C_2 from the one in C_3, and so on. $\Delta C21$, $\Delta C32$, $\Delta C43$ and $\Delta C54$ are respectively 0.25 °C, 0.18 °C, 0.47 °C and 0.53 °C for all of China. Their increasing rates are respectively 4 %, 3 %, 6 % and 7 %.
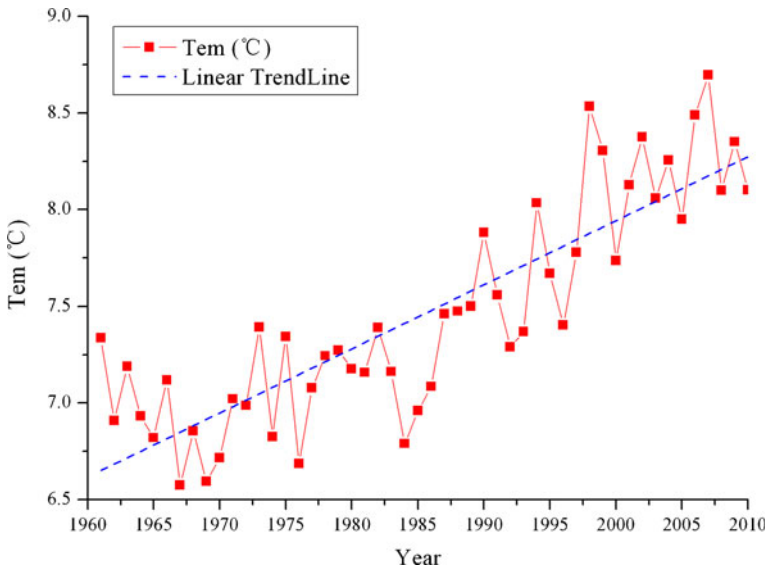
Fig. 2 Time series of annual average temperature from 1961 to 2010

The simulation results in terms of HASM-OLS indicate that on a cell-by-cell basis, each sub-period showed either warming or cooling. During the period from C_1 to C_2, the percentage of 1 km grid cells that had an increasing trend of MAT (PGCIT) was 75 % for the entire landmass of China. On a regional basis, all 9 regions had warming trends except for R_9 which had a cooling trend. R_4 had the biggest PGCIT of 95 %, while R_9 had the smallest PGCIT of 18 %. R_5 had the biggest increase of MAT from C_1 to C_2 on average (Fig. 3). From C_2 to C_3, PGCIT was 77 % and MAT increased an average of 0.18 °C for the entire landmass of China. The increasing rate was 3 %. Except for a cooling trend in R_6 for this period, all other regions had a warming trend. The highest warming rate was in R_3. From C_3 to C_4, PGCIT was 94 %; the rise in MAT was 0.47 °C across China, with a rate of increase of 6 %. R_1 had the largest PGCIT and the highest rise in MAT; R_6 had the smallest PGCIT and the lowest rise in MAT. From C_4 to C_5, PGCIT was 88 %; MAT rose 0.53 °C with an average warming rate of 7 % across China. R_9 had the largest PGCIT and R_5 had the highest increase in MAT.

Except the cooling trend in the sub-period from C_1 to C_2 in R_9 and from C_2 to C_3 in R_6, all other regions in China for all other sub-periods had a warming trend. Especially in R_5, Qinghai-Xizang plateau, MAT increased by 1.91 °C with a warming rate of 443 % in last 50 years. MAT in regions of R_1, R_2, R_3 and R_4 increased by 1.61, 1.68, 1.37 and 1.27 °C with rising rates of 42 %, 27 %, 79 % and 14 % respectively, while there were lower warming rates in the regions of R_6, R_7, R_8 and R_9. MAT in these regions were higher 0.73, 0.77, 0.98 and 0.92 °C in the last 50 years, with warming rates of 5 %, 4 %, 7 % and 5 % respectively.
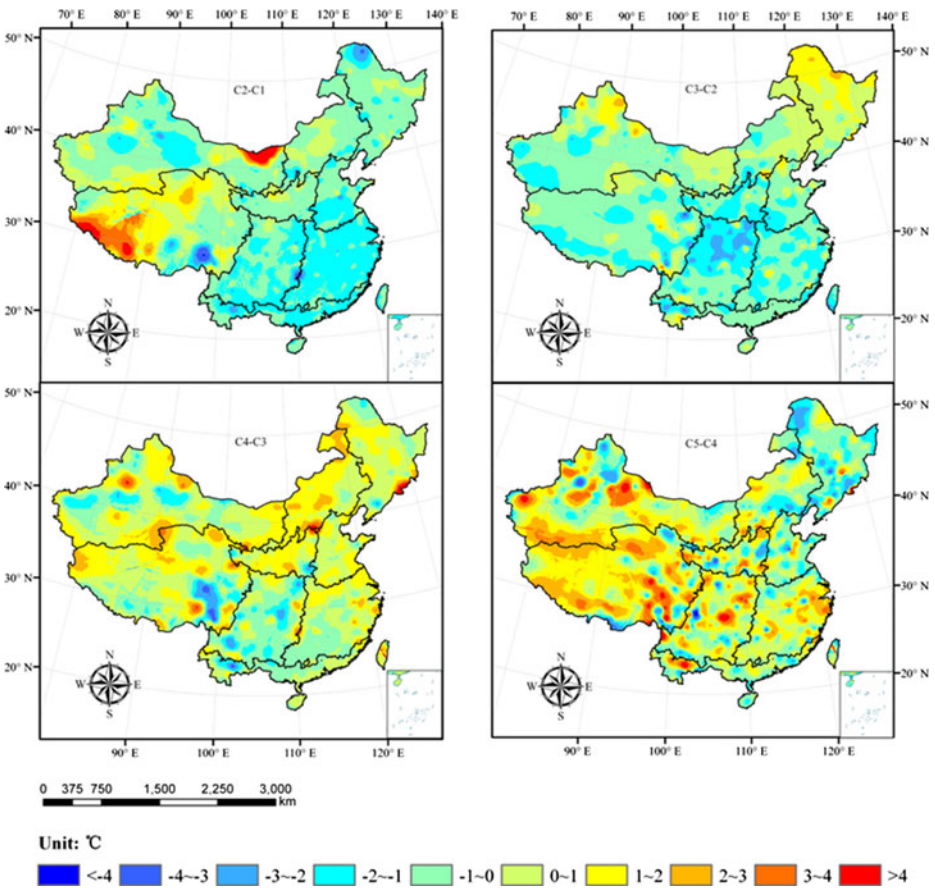
3.2 Mean annual precipitation

MAP averaged 583.78, 585.16, 591.08, 593.03 and 585.78 mm for the decadal sub-periods of C_1, C_2, C_3, C_4 and C_5 respectively across China. MAP increased by 1.39, 5.93 and 1.93 mm

Table 3 Change trends of MAT during the 1961 to 2010 period for the 9 regions of China

| Region		R_1	R_2	R_3	R_4	R_5	R_6	R_7	R_8	R_9	The whole land of China
From C_1 to C_2	MAT in C_1	3.33	5.68	1.61	8.31	-0.33	14.44	20.11	12.89	16.61	6.91
	$\Delta C21$ (°C)	0.23	0.34	0.14	0.19	0.56	0.02	0.00	0.04	-0.09	0.25
	Changing rate (%)	7	6	9	2	170	0	0	0	-1	4
	PGCIT (%)	94	85	85	95	93	56	48	58	18	75
From C_2 to C_3	MAT in C_2	3.57	6.11	1.75	8.49	0.24	14.45	20.11	12.93	16.51	7.15
	$\Delta C32$ (°C)	0.30	0.23	0.57	0.02	0.14	-0.08	0.06	0.14	0.04	0.18
	Changing rate (%)	8	4	33	0	59	-1	0	1	0	3
	PGCIT (%)	92	87	100	52	78	42	74	77	66	77
From C_3 to C_4	MAT in C_3	3.87	6.34	2.33	8.50	0.37	14.37	20.18	13.07	16.52	7.33
	$\Delta C43$ (°C)	0.72	0.48	0.55	0.61	0.46	0.23	0.32	0.53	0.43	0.47
	Changing rate (%)	19	8	24	7	124	2	2	4	3	6
	PGCIT (%)	100	92	98	95	91	83	91	99	100	94
From C_4 to C_5	MAT in C_4	4.60	6.81	2.87	9.10	0.85	14.59	20.49	13.62	16.97	7.82
	$\Delta C54$ (°C)	0.36	0.63	0.11	0.45	0.75	0.56	0.39	0.27	0.54	0.53
	Changing rate (%)	8	9	4	5	90	4	2	2	3	7
	PGCIT (%)	84	92	63	83	94	92	89	82	95	88

Fig. 3 Changes in MAT from 1960s to 2000s

from C_1 to C_2, from C_2 to C_3 and from C_3 to C_4 respectively, while decreasing by 7.25 mm from C_4 to C_5. In Table 4, $\Delta C21$ represents the result of subtracting the value of MAP in C_1 from the value of the MAP in C_2, $\Delta C32$ represents the result of subtracting the value of the MAP in C_2 from the one in C_3, and so on.

Simulation results of HASM-GWR-BC indicate that portions of all 9 regions and all 5 sub-periods showed both increased and decreased precipitation. From C_1 to C_2, 55 % of China showed an increasing trend in MAP (PGCIP); MAP increased by 1.39 mm across China on average and the increasing rate approached to 0. R_5 had the largest PGCIP and the highest increasing rate. R_4 the smallest PGCIP and the highest decrease in MAP. R_7 had the highest increase in MAP (Fig. 4). From C_2 to C_3, PGCIP was 59 % and MAP increased by 5.93 mm at an average rate of 1 % across China. R_3 had the biggest PGCIP, the highest increase in MAP and the largest increasing rate. R_8 exhibited the smallest PGCIP, the largest decrease of MAP and the biggest decreasing rate. From C_3 to C_4, PGCIP was 53 %; MAP increased by 1.93 mm with an average rate approaching 0 across China. R_9 had the biggest PGCIP and the highest rise in MAP. R_2 had the largest increasing rate. The smallest PGCIP appeared in R_4. R_4 exhibited the deepest drop in MAP and the largest decreasing rate. From C_4 to C_5, PGCIP was 53 % and MAP decreased by −7.25 mm, at a rate of −1 %, across China. R_4 had the largest PGCIP. R_8 had

Table 4 Change trends of MAP during the 1961 to 2010 period for the 9 regions of China

Region		R_1	R_2	R_3	R_4	R_5	R_6	R_7	R_8	R_9	The whole land of China
From C_1 to C_2	MAP (mm) in C_1	324.60	117.44	547.12	529.77	371.80	1037.60	1465.40	734.78	1414.95	583.78
	$\Delta C21$ (mm)	-3.34	3.15	-25.08	-43.45	19.60	-22.95	47.34	-18.74	15.3	1.39
	Changing rate (%)	-1	3	-5	-8	5	-2	3	-3	1	0
	PGCIP (%)	55	71	15	5	86	18	64	11	58	55
From C_2 to C_3	MAP (mm) in C_2	321.26	120.58	522.03	486.31	391.39	1014.60	1512.71	716.03	1430.30	585.16
	$\Delta C32$ (mm)	6.32	3.71	91.80	15.19	5.27	-4.96	-13.56	-46.62	3.44	5.93
	Changing rate (%)	2	3	18	3	1	-1	-1	-7	0	1
	PGCIP (%)	45	61	98	68	59	57	44	14	58	59
From C_3 to C_4	MAP (mm) in C_3	327.57	124.28	613.82	501.49	396.65	1009.64	1499.14	669.45	1433.75	591.08
	$\Delta C43$ (mm)	3.57	8.58	-29.92	-54.11	2.75	-39.48	16.87	6.53	71.49	1.93
	Changing rate (%)	1	7	-5	-11	1	-4	1	1	5	0
	PGCIP (%)	57	76	7	4	45	37	72	58	83	53
From C_4 to C_5	MAP (mm) in C_4	331.15	132.85	549.36	447.40	399.43	970.21	1516.06	675.97	1505.18	593.03
	$\Delta C54$ (mm)	-48.33	5.42	-32.30	24.23	24.93	5.34	-24.82	38.15	-89.62	-7.25
	Changing rate (%)	-14	4	-6	5	6	1	-2	6	-6	-1
	PGCIP (%)	8	60	15	88	87	62	27	79	11	53
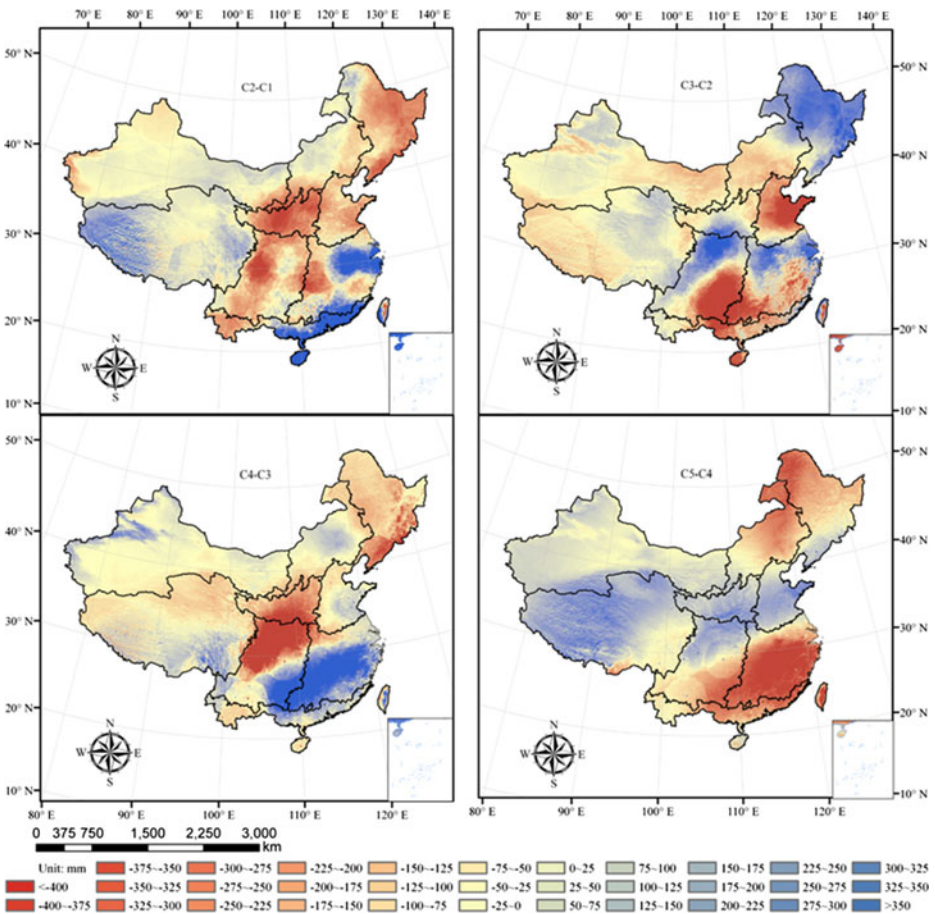
Fig. 4 Changes in MAP from 1960s to 2000s

the biggest increase in MAP. R_1 had the smallest PGCIP and the deepest dropping rate. R_9 had the deepest drop in MAP.

Since 1960s, MAP in R_5 and R_2 has had a continuously increasing trend; MAP increased by 52.55 and 20.86 mm with the increasing rates of 13 % and 17 % in recent 50 years respectively. In other 7 regions, MAP has been variably changed and increasing MAP alternated with decreasing MAP. On average, MAP in the regions of R_1, R_4, R_6 and R_8 decreased by 41.78, 58.14, 62.05 and 20.68 mm, with changing rates of −12 %, −11 %, −6 % and −3 % respectively, in recent 50 years; in R_3, R_7 and R_9, MAP increased by 4.5, 25.83 and 0.61 mm, with rising rates of 2 %, 1 % and 0.

4 Maximum differences among different regions and periods

4.1 MAT

In order to discuss the maximum differences of MAT among different regions and periods, we introduce the following indexes for maximum warming rate (MWR), maximum warming

amplitude (MWA), maximum cooling rate (MCR) and maximum cooling amplitude (MCA) as follows,

$$MWR(R_i, C_t) = \max_{(j,k)\in Ri} \left\{ \frac{MAT_{j,k}(R_i, C_{t+1}) - MAT_{j,k}(R_i, C_t)}{MAT_{j,k}(R_i, C_t)} \times 100\% \right\} \quad (6)$$

$$MWA(R_i, C_t) = \max_{(j,k)\in R_i} \left\{ MAT_{j,k}(R_i, C_{t+1}) - MAT_{j,k}(R_i, C_t) \right\} \quad (7)$$

$$MCR(R_i, C_t) = \max_{(j,k)\in R_i} \left\{ \frac{MAT_{j,k}(R_i, C_t) - MAT_{j,k}(R_i, C_{t+1})}{MAT_{j,k}(R_i, C_t)} \times 100\% \right\} \quad (8)$$

$$MCA(R_i, C_t) = \max_{(j,k)\in R_i} \left\{ MAT_{j,k}(R_i, C_t) - MAT_{j,k}(R_i, C_{t+1}) \right\} \quad (9)$$

where $(j, k)\in R_i$ means that (j, k) is any grid cell in the region of R_i, $i=1,2,\ldots,9$; $MAT_{j,k}(R_i, C_t)$ represents the mean annual temperature at grid cell (j, k) in the sub-period C_t, $t=1,2,3,4$.

In light of changing rates (Table 5), from C_1 to C_2, the MWRs greater than 300 % appeared in northeastern R_2 and western R_5, respectively with MWRs of 447 % and 337 % as well as MWAs of 5.01 °C and 3.64 °C; the biggest MCR, 66 %, happened in northern R_3, with a MCA of 1.22 °C. From C_2 to C_3, the biggest MWR was 136 %, appearing in southeastern R_3 with a MWA of 1.74 °C; the biggest MCR of 223 %, with a MCA of 1.58 °C, was in the eastern R_5. From C_3 to C_4, the biggest MWR was 340 % in western R_2,

Table 5 Maximum differences of MAT among different regions and periods

Region		R_1	R_2	R_3	R_4	R_5	R_6	R_7	R_8	R_9
From C_1 to C_2	MWA (°C)	0.88	5.01	0.67	0.77	3.64	0.7	0.46	1.21	0.38
	MWR (%)	19	447	46	10	337	12	4	15	3
	MCA (°C)	0.66	0.63	1.22	0.67	3.33	2.03	0.78	0.85	1.86
	MCR (%)	8	5	66	8	50	13	3	11	13
From C_2 to C_3	MWA (°C)	1.44	1.28	1.74	1.46	1.77	1.02	1.47	1.18	0.84
	MWR (%)	66	66	136	25	25	8	8	14	6
	MCA (°C)	0.6	0.46	0.18	0.62	1.58	0.94	1.32	0.47	0.36
	MCR (%)	8	4	5	8	223	6	11	3	3
From C_3 to C_4	MWA (°C)	3.09	2.45	4.5	3.09	2.31	1.93	2.53	2.11	2.27
	MWR (%)	140	340	276	46	120	13	20	26	15
	MCA (°C)	0.04	0.51	0.66	0.95	1.59	1.02	1.52	0.45	0.28
	MCR (%)	1	6	10	7	20	7	7	3	2
From C_4 to C_5	MWA (°C)	1.79	3.5	4.7	1.76	3.81	4.98	3.76	1.49	2.22
	MWR (%)	30	37	101	14	57	30	16	11	15
	MCA (°C)	0.92	2.47	1.58	2.43	1.67	2.54	1.74	2.58	1.46
	MCR (%)	103	229	27	38	43	22	9	24	8

with a MWA of 2.45 °C, and the largest MCA was 1.59 °C, with the biggest MCR of 20 % in southeastern R_5. From C_4 to C_5, the biggest MWR, 101 %, was found in southeastern R_3, with a MWA of 4.7 °C; the largest MCR, 229 %, happened in western R_2 and the MCA was 2.47 °C.

In terms of changing amplitudes of MAT, the biggest MWAs were 5.01 °C in northeastern R_2, 1.77 °C in southeastern R_5, 4.5 °C in southeastern R_3, and 4.98 °C in southeastern R_6 respectively in the sub-periods from C_1 to C_2, from C_2 to C_3, from C_3 to C_4 and from C_4 to C_5. The highest MCAs were 3.33 °C in southeastern R_5, 1.58 °C in eastern R_5, 1.59 °C in southeastern R_5, and 2.58 °C in the middle of R_8 in the same sub-periods.

4.2 MAP

Indexes of maximum wetter rate (MWER), maximum wetter amplitude (MWEA), maximum drier rate (MDR) and maximum drier amplitude (MDA) are formulated as follows,

$$MWER(R_i, C_t) = \max_{(j,k)\in Ri} \left\{ \frac{MAP_{j,k}(R_i, C_{t+1}) - MAP_{j,k}(R_i, C_t)}{MAP_{j,k}(R_i, C_t)} \times 100\% \right\} \qquad (10)$$

$$MWEA(R_i, C_t) = \max_{(j,k)\in R_i} \left\{ MAP_{j,k}(R_i, C_{t+1}) - MAP_{j,k}(R_i, C_t) \right\} \qquad (11)$$

$$MDR(R_i, C_t) = \max_{(j,k)\in R_i} \left\{ \frac{MAP_{j,k}(R_i, C_t) - MAT_{j,k}(R_i, C_{t+1})}{MAP_{j,k}(R_i, C_t)} \times 100\% \right\} \qquad (12)$$

$$MDA(R_i, C_t) = \max_{(j,k)\in R_i} \left\{ MAP_{j,k}(R_i, C_t) - MAP_{j,k}(R_i, C_{t+1}) \right\} \qquad (13)$$

where $(j, k) \in R_i$ means that (j, k) is any grid cell in the region of R_i, $i=1,2,\dots,9$; $MAP_{j,k}(R_i, C_t)$ represents the mean annual precipitation at grid cell (j, k) in the sub-period C_t, $t=1,2,3,4$.

The biggest value of MWER was 47 % in the sub-period from C_1 to C_2 and happened in southwestern R_5, 47 % from C_2 to C_3 in southern R_2, 48 % from C_3 to C_4 in southwestern R_2, and 89 % from C_4 to C_5 in southwestern R_3. From C_1 to C_2, the largest MDR was 32 %, which was found in western R_2; from C_2 to C_3, it was 18 % in southwestern R_8; from C_3 to C_4, it was 82 % in southwestern R_3; from C_4 to C_5, the highest MDR appeared in the middle of R_1 (Table 6).

The biggest WMEAs were 276.69 mm in the sub-period from C_1 to C_2 appearing in southern Hainan province of R_7, 177.71 mm from C_2 to C_3 in southeastern R3; 335.66 mm from C_3 to C_4 in southeastern R_9, and 762.00 mm from C_3 to C_4 in the middle of R_6. The highest MDA was 145.98 mm in the southeastern Hainan province of R_7, 253.20 mm in southwestern R_7, 723.98 mm in southwestern R_6 and 474.91 mm in southeastern R_9 in the sub-periods from C_1 to C_2, from C_2 to C_3, from C_3 to C_4 and from C_4 to C_5 respectively.

Table 6 Maximum differences of MAP among different regions and periods

Region		R_1	R_2	R_3	R_4	R_5	R_6	R_7	R_8	R_9
From C_1 to C_2	MWEA (mm)	39.92	43.69	61.84	37.13	149.23	53.21	276.69	40.77	157.35
	MWER (%)	13	23	18	7	47	8	19	5	11
	MDA (mm)	69.34	66.23	91.70	80.84	42.94	100.74	145.98	73.22	109.09
	MDR (%)	19	32	10	16	13	9	8	9	7
From C_2 to C_3	MWEA (mm)	72.21	39.92	177.71	95.68	57.68	116.63	119.46	94.96	112.26
	MWER (%)	19	47	9	14	7	16	7	10	10
	MDA (mm)	42.47	45.39	65.33	33.12	63.44	176.92	253.20	131.92	228.03
	MDR (%)	8	15	10	10	16	14	14	18	11
From C_3 to C_4	MWEA (mm)	71.01	140.25	72.66	46.32	153.84	288.31	238.95	159.18	335.66
	MWER (%)	13	48	15	12	24	22	14	24	20
	MDA (mm)	135.82	43.44	693.91	176.27	229.67	723.98	254.67	160.87	493.48
	MDR (%)	40	17	82	22	47	63	13	18	28
From C_4 to C_5	MWEA (mm)	58.01	66.81	650.66	128.23	289.52	762.00	158.34	305.71	476.73
	MWER (%)	16	32	89	21	36	69	9	60	26
	MDA (mm)	116.52	47.8	130.95	47.45	118.92	301.44	230.99	202.45	474.91
	MDR (%)	36	14	28	9	23	20	12	21	29

5 Conclusions

Topography of land in China from Qinghai-Xizang plateau eastward, is broadly arranged into three great steps (Zhao 1986). The first step is Qinghai-Xizang plateau, with mean elevation above 4,000 m; the second step is from the eastern margin of Qinghai-Xizang plateau eastward up to Da Hinggan-Taihang-Wushan mountains line, with elevations from 2,000 to 1,000 m; the third step is from the above-mentioned line eastward up to the coast, below 500 m in elevation (Fig. 1). The warming rates increase from south to north in the second and third steps of China. In particular, the 2,100 °C d contour line of annual accumulated temperature (AAT) of ≥10 °C in Heilongjiang province of R3 shifted northwestward 255 km since the 1960s (Supplement 4). Areas suitable for planting early rice expanded about 3.8 million hectares because of the AAT change. The 2,400 °C d contour line of ≥10 °C AAT moved northward at least 167 km since 1960, which made the area suitable for planting early maize increase by about 5.5 million hectares in Heilongjiang province.

MAT had an increasing trend during the period from 1960 to 2010 in China, with an especially accelerating increase trend since the 1980s. MAT was respectively 6.91 °C, 7.15 °C、7.33 °C, 7.82 °C and 8.35 °C during the sub-periods of C_1, C_2, C_3, C_4 and C_5. The increasing rates of MAT were respectively 4 %, 3 %, 6 % and 7 % during the sub-periods from C_1 to C_2, from C_2 to C_3, from C_3 to C_4 and from C_4 to C_5. The biggest values of MWRs and MCRs appeared in the regions of R_1, R_2, R_3 and R_5 in the four sub-periods. According to both changing rates and amplitudes, Qinghai-Xizang Plateau and Northern China had more extremes of temperature than Southern China since the 1960s.

MAP was 583.78 mm in C_1, 585.16 mm in C_2, 591.08 mm in C_3, 593.03 mm in C_4 and 585.78 mm in C_5. MAP increased by 1.39 mm from C_1 to C_2, by 5.93 mm from C_2 to C_3, and by 1.93 mm from C_3 to C_4, while MAP decreased by 7.254 mm from C_4 to C_5. On average, China became wetter during the period from 1960s to 1990s, but much drier from 1990s to 2000s. Since the 1960s, MAP in Qinghai-Xizang plateau and in arid region has had a continuously increasing trend, with the increasing rates of 13 % and 17 % in recent 50 years respectively. In other regions, increasing MAP alternated with decreasing MAP decade by decade.

In terms of changing rates, north China and Qinghai-Xizang plateau had more extremes of precipitation in the last five decades. According to changing amplitudes, South China and Sichuan basin had more extremes of precipitation.

References

Agnew MD, Palutikof JP (2000) GIS-based construction of baseline climatologiesfor the Mediterranean using terrain variables. Clim Res 14:115–127

Akinyemi FO, Adejuwon JO (2008) A GIS-based procedure for downscaling climate data for west Africa. Trans GIS 12(5):613–631

Ashiq MW, Zhao CY, Ni J, Akhtar M (2010) GIS-based high-resolution spatial interpolation of precipitation in mountain–plain areas of Upper Pakistan for regional climate change impact studies. Theor Appl Climatol 99:239–253

Hancock PA, Hutchinson MF (2006) Spatial interpolation of large climate data sets using bivariatethin plate smoothing splines. Environ Model Softw 21:1684–1694

Hong Y, Nix HA, Hutchinson MF, Booth TH (2005) Spatial interpolation of monthly mean climate data for China. Int J Climatol 25:1369–1379

Jeffrey SJ, Carter JO, Moodie KB, Beswick AR (2001) Using spatial interpolation to construct a comprehensive archive of Australian climate data. Environ Model Softw 16:309–330

Lin ZH, Muo XG, Li HX, Li HB (2002) Comparison of three spatial interpolation methods for climate variables in China. Acta Geograph Sin 57:47–56 (in Chinese)

Lloyd CD (2005) Assessing the effect of integrating elevation data into the estimation of monthly precipitation in Great Britain. J Hydrol 308:128–150

Pan YZ, Gong DY, Deng L, Li J, Gao J (2004) Smart distance searching based and DEM informed interpolation of surface air temperature in China. Acta Geograph Sin 59:366–374 (in Chinese)

Ruelland D, Ardoin-Bardin S, Billen G, Servat E (2008) Sensitivity of a lumped and semi-distributed hydrological model to several methods of rainfall interpolation on a large basin in West Africa. J Hydrol 361:96–117

Samanta S, Pal DK, Lohar D, Pal B (2012) Interpolation of climate variables and temperature modeling. Theor Appl Climatol 107:35–45

Shang ZB, Guo Q, Yang DA (2001) Spatial pattern analysis of annual precipitation with climate information system of China. Acta Ecol Sin 21:689–694 (in Chinese)

Yue TX (2011) Surface Modelling: High Accuracy and High Speed Methods. CRC Press, New York

Zhao SQ (1986) Physical Geography of China. John Wiley & Sons, New York

Zhou LS, Sun H, Shen YQ, Deng JZ, Shi YL (1981) Comprehensive Agricultural Planning of China. China Agricultural Press, Beijing (in Chinese)